

# ENERGY SPREAD CONSTRAINTS ON FIELD SUPPRESSION IN A REVERSE TAPERED UNDULATOR\*

J. MacArthur, A. Marinelli, A. Lutman, H.-D. Nuhn, Z. Huang  
SLAC National Accelerator Laboratory, Menlo Park, CA, USA

## Abstract

A 3.2 m variable polarization Delta undulator [1] has been installed at the end of the LCLS undulator line. The Delta undulator acts as an afterburner in this configuration, using bunching from upstream planar undulators to produce radiation with arbitrary polarization. To optimize the degree of polarization from this device, a reverse taper has been proposed [2] to suppress background radiation produced in upstream undulators while still microbunching the beam. Here we extend previous work on free electron lasers with a slowly varying undulator parameter [3] to show there is a strong energy spread dependence to the maximum allowable detune from resonance. At LCLS, this energy spread limitation keeps the reverse taper slope in the slowly varying regime and limits the achievable degree of circular polarization.

## INTRODUCTION

Circularly polarized x-rays can be used to probe ultrafast demagnetization processes [4], image nanoscale spin order [5], and probe the chirality of biomolecules [6]. However, no x-ray Free Electron Lasers (FELs) offer direct production of circular x-rays. A helical undulator called the Delta undulator is being commissioned at the Linac Coherent Light Source (LCLS) to address this shortcoming [7].

The Delta undulator is not long enough to operate alone and reach appreciable power levels. The electron beam must therefore be prepared in advance of the Delta undulator to maximize the power produced in the circular polarization mode. A reverse tapered planar undulator line preceding the Delta undulator was proposed [2] to maximize the microbunching in a beam entering the Delta undulator while suppressing the background linear field. In this paper we present a constraint on the effectiveness of the reverse taper technique in FELs with a relatively large energy spread.

In the following sections, the 1D FEL equations are explored in the slowly varying detune regime. For an undulator of period  $\lambda_u$ , Pierce parameter  $\rho$ , and  $z$ -dependent resonant energy  $\gamma_r(z)$ , the detune from the initial energy  $\gamma_0$  is

$$\delta = \frac{\gamma_0 - \gamma_r(z)}{\gamma_0}. \quad (1)$$

The detune is slowly varying when its change over a gain length  $L_G \approx \lambda_u/4\pi\rho$  is significantly less than the gain bandwidth, which is typically several  $\rho$  [3]. Thus the slowly

varying technique is valid when

$$\frac{\lambda_u}{4\pi\rho} \left| \frac{d\delta}{dz} \right| < \rho. \quad (2)$$

At LCLS, successful 720 eV reverse taper configurations operate with a maximum reverse taper detune of  $\delta = -0.005$  applied over six undulator modules, or 20 m. These conditions mandate a Pierce parameter satisfying

$$\rho > \sqrt{\frac{\lambda_u}{4\pi} \left| \frac{d\delta}{dz} \right|} = 7.7 \times 10^{-4}. \quad (3)$$

Typical 720 eV reverse taper runs operate at a peak current of 5 kA with a 30  $\mu\text{m}$  transverse beam size, resulting in a Pierce parameter of  $2.2 \times 10^{-3}$ . It is therefore instructive to apply the slowly varying solution of the FEL equations to soft x-ray experiments at LCLS.

In the following section we review important aspects of FELs with slowly varying parameters. In subsequent sections we apply this formalism to a reverse tapered undulator to calculate an energy spread limit on the effectiveness of a reverse tapered undulator line. Finally, 3D simulations are compared with results from the 1D theoretical framework.

## WKB REVIEW

The Vlasov and Maxwell equations can be expressed in matrix form [3],

$$\frac{d}{d\bar{z}} \begin{pmatrix} a_v \\ f_v \end{pmatrix} = iM \begin{pmatrix} a_v \\ f_v \end{pmatrix}, \quad (4)$$

$$M = \begin{pmatrix} -\bar{v} & -i \int_{-\infty}^{\infty} d\bar{\eta} \\ -i \frac{d\bar{v}}{d\bar{\eta}} & -(\bar{\eta} - \bar{\delta}) \end{pmatrix}. \quad (5)$$

The dimensionless FEL variables used here are

$$\bar{z} = 2\rho k_u z \quad (6)$$

$$\bar{\eta} = \frac{\gamma(z) - \gamma_c(z)}{\gamma_0\rho} \quad (7)$$

$$\bar{\delta} = \frac{\gamma_c(z) - \gamma_r(z)}{\gamma_0\rho} \quad (8)$$

$$\bar{v} = \frac{\Delta v}{2\rho} \quad (9)$$

$$a_v = -\frac{eK[\text{JJ}]}{4\gamma_0^2 m c^2 k_u \rho} e^{-i\Delta v k_u z} E_v \quad (10)$$

$$f_v = \frac{2k_u \rho^2}{k_0} F_v, \quad (11)$$

where  $\rho$  and  $k_u$  are the Pierce parameter and undulator wavenumber. The Lorentz factor  $\gamma_0$  defines the mean beam

\* Work supported by U.S. DOE Office of Basic Energy Sciences under Contract No. DE-AC02-76SF00515.

energy at the start of the undulator line, while  $\gamma_c(z)$  and  $\gamma_r(z)$  represent the mean beam energy in the absence of FEL interaction and the beam energy resonant with the rms undulator parameter value  $a_u(z)$ ,

$$\gamma_r(z) = \sqrt{\frac{k_0}{2k_u} (1 + a_u(z)^2)} \quad (12)$$

The radiation wavenumber resonant at the start of the undulator line is  $k_0$ . In an undulator line in a reverse taper configuration,  $a_u$  increases with  $z$ .

The frequency detune is  $\Delta\nu = (k - k_0)/k_0 = \nu - 1$ , where  $k$  is the radiation wavenumber. The Fourier component of the electric field is  $E_\nu$ . The electron energy distribution is represented by a smooth distribution  $V(\eta)$  and a microbunched perturbation  $\delta F(\theta, \eta, z)$ . The Fourier component of the of the distribution function is

$$F_\nu = \frac{1}{2\pi} \int \delta F(\theta, \eta, z) e^{-i\nu\theta} d\theta, \quad (13)$$

which can be integrated to give the bunching parameter

$$b_\nu = \int F_\nu d\eta. \quad (14)$$

Eq. (4) has been solved in the case of a slowly varying  $\bar{\delta}(z)$  to be of the form

$$\begin{pmatrix} a_\nu \\ f_\nu \end{pmatrix} = \Psi_0 \exp\left(-i \int_0^z (\mu_0(\tau) + \mu_1(\tau)) d\tau\right), \quad (15)$$

where  $\mu_0$  is the zeroth order growth rate and  $\mu_1$  is a small first order correction. The eigenvector  $\Psi_0$  is

$$\Psi_0(z) \propto \begin{pmatrix} 1 \\ \frac{i}{\mu_0 - (\bar{\eta} - \bar{\delta})} \frac{dV}{d\bar{\eta}} \end{pmatrix}. \quad (16)$$

With the change of variables

$$\hat{\mu} = \mu_0 - \bar{\delta} \quad (17)$$

$$\hat{\nu} = \bar{\nu} - \bar{\delta}, \quad (18)$$

the zeroth order growth rate satisfies

$$\hat{\mu} - \hat{\nu} = \int_{-\infty}^{\infty} \frac{d\bar{\eta}}{\bar{\eta} - \hat{\mu}} \frac{dV}{d\bar{\eta}} \quad (19)$$

The imaginary part of  $\hat{\mu}$  and leads to exponential field growth. In subsequent sections we ignore the imaginary part of  $\mu_1$  as it is small and negative in a reverse tapered undualtor [3].

## UPPER BOUND ON THE DETUNE

Given an energy distribution  $V(\bar{\eta})$ , the growth rate  $\text{Im}(\hat{\mu})$  can be calculated numerically. The growth rate is typically largest at a small negative  $\hat{\nu}$ . In a reverse taper, however,  $\bar{\delta}$  may take on large negative values, leading to a large positive  $\hat{\nu}$ . If  $\hat{\nu}$  is too large, the imaginary part of  $\hat{\mu}$  reaches zero, killing the FEL interaction. In this section we explore the energy spread dependent limit on the combined detune  $\hat{\nu}$ .

For a Gaussian beam with an energy standard deviation of  $\zeta$ ,  $V(\bar{\eta})$  takes the form

$$V(\bar{\eta}) = \frac{1}{\sqrt{2\pi}\zeta} e^{-\bar{\eta}^2/2\zeta^2}. \quad (20)$$

Using this energy distribution, Eq. (19) can be expressed in terms of the error function  $\text{erf}(x)$ ,

$$\hat{\mu} - \hat{\nu} = -\frac{1}{\zeta^2} - i\sqrt{\frac{\pi}{2}} \frac{\hat{\mu}}{\zeta^3} e^{-\hat{\mu}^2/2\zeta^2} \left(1 + \text{erf}\left(\frac{i\hat{\mu}}{\sqrt{2}\zeta}\right)\right), \quad (21)$$

where

$$\text{erf}(x) = \frac{2}{\sqrt{\pi}} \int_0^x e^{-t^2} dt. \quad (22)$$

FEL growth stops when  $\text{Im}(\hat{\mu}) = 0$ . The detune  $\hat{\nu}$  and energy spread  $\zeta$  are purely real, so FEL growth stops when

$$0 = \text{Re} \left[ \hat{\mu} e^{-\hat{\mu}^2/2\zeta^2} \left(1 + \text{erf}\left(\frac{i\hat{\mu}}{\sqrt{2}\zeta}\right)\right) \right] \quad (23)$$

However, the error function is purely imaginary for purely imaginary argument, so Eq. (23) implies  $\text{Re}(\hat{\mu}) = \text{Im}(\hat{\mu}) = 0$ . Referring back to Eq. (21), this implies the upper limit on  $\hat{\nu}$  at a given energy spread  $\zeta$  is simply

$$\hat{\nu} \leq \frac{1}{\zeta^2}. \quad (24)$$

A contour plot of  $\text{Im}(\hat{\mu})$  is shown as a function of the scaled energy spread and detune in Fig. 1. The  $\text{Im}(\hat{\mu}) = 0$  contour is parameterized by  $\hat{\nu} = 1/\zeta^2$ , as denoted by the dotted line.

Table 1: Distribution Dependent  $\hat{\nu}$  Boundary

$V(\bar{\eta})$	Width (rms)	Boundary
Eq. (20)	$\zeta$	$\hat{\nu} = 1/\zeta^2$
Eq. (A5)	$\zeta$	$\hat{\nu} = 1/2\zeta^2$

X-ray FEL's often use a laser heater to combat the microbunching instability [8]. The laser heater imparts a non-Gaussian energy spread on an initially Gaussian beam, modifying  $V(\bar{\eta})$ . If the pre-laser heater energy spread is inordinably small, the  $\hat{\nu}$  boundary still takes a simple form. Coincidentally, as observed by one of us<sup>1</sup>, the growth rate itself resulting from a matched laser heater is algebraic. These results are discussed in the appendix. Table 1 presents a summary, where the energy spread dependent upper limit on the detune is reported for FEL's operation with different energy distributions.

<sup>1</sup> A. Marinelli

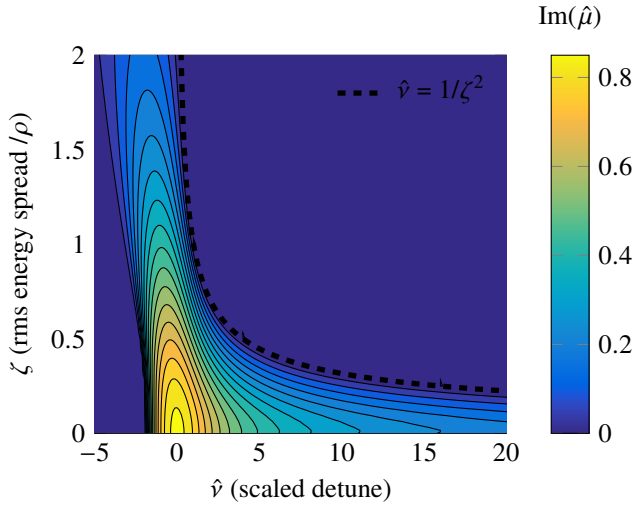


Figure 1: A numerical calculation of the growth rate  $\text{Im}(\hat{\mu})$  as a function of the scaled detune  $\hat{\nu}$  and the scaled rms energy spread  $\zeta$ . FEL's with a finite energy spread operate most efficiently with a small negative  $\hat{\nu}$  (yellow, green). However, a reverse tapered FEL may operate near the  $\text{Im}(\hat{\mu}) = 0$  boundary. This boundary is parametrized by Eq. (24). In this calculation the energy distribution is assumed to be Gaussian with a standard deviation of  $\zeta$ .

## IMPLICATIONS FOR REVERSE TAPER EXPERIMENTS

The purpose of a reverse tapered undulator line is to suppress the field growth relative to the bunching. At a given frequency  $\nu$ , this means

$$\left| \frac{b_\nu}{a_\nu} \right| \gg 1 \quad (25)$$

is desirable. In this section, we relate this condition to the scaled detune  $\hat{\nu}$ .

Using the definition of  $b_\nu$  given in Eq. (14) and the evolution of  $f_\nu$  and  $a_\nu$  shown in Eqs. (15,16), the ratio of the bunching factor to the field is

$$\left| \frac{b_\nu}{a_\nu} \right| = \left| \frac{\int d\bar{\eta} \exp(-i \int_0^{\bar{z}} (\mu_0 + \mu_1) d\tau) \frac{1}{\bar{\eta} - \hat{\mu}} \frac{dV}{d\bar{\eta}}}{\exp(-i \int_0^{\bar{z}} (\mu_0 + \mu_1) d\tau)} \right| \quad (26)$$

$$= \left| \int \frac{d\bar{\eta}}{\bar{\eta} - \hat{\mu}} \frac{dV}{d\bar{\eta}} \right|, \quad (27)$$

which can be simplified with the dispersion relation in Eq. (19),

$$\left| \frac{b_\nu}{a_\nu} \right| = |\hat{\mu} - \hat{\nu}|. \quad (28)$$

Evidently, the ratio of the bunching to the field at a given location along the undulator line depends only on the present detune and growth parameter. As long as the slowly varying approximation is satisfied,  $|b_\nu/a_\nu|$  is independent of the taper history.

Often the magnitude of  $\hat{\mu}$  is close to zero, so  $|\hat{\nu}| \gg |\hat{\mu}|$  for a large detune. In fact  $\hat{\mu}$  is exactly zero on the boundary discussed in the previous section. Therefore a large scaled detune  $\hat{\nu}$  means

$$\left| \frac{b_\nu}{a_\nu} \right| \approx \hat{\nu}. \quad (29)$$

As seen in previous section, the energy spread places an upper limit on  $\hat{\nu}$ . This upper limit transfers to the present situation,

$$\left| \frac{b_\nu}{a_\nu} \right| \leq \frac{1}{\zeta^2} = \frac{\rho^2 \gamma_0^2}{\sigma_\gamma^2}, \quad (30)$$

where  $\sigma_\gamma$  is the rms beam energy spread in units of  $m_e c^2$ . A beam with a relatively large energy spread cannot suppress the field strength relative to the bunching strength.

## 3D SIMULATION

In a SASE FEL with a reverse tapered undulator, the bunching and field evolve over a range of frequencies. The framework presented above is relevant for a particular frequency  $\nu$ , but it can help explain the bunching evolution in a 3D reverse taper simulation with a large energy spread.

In Fig. 2, the bunching spectrum evolution during two time-dependent Genesis simulations is shown. Both simulations were done in a reverse tapered undulator, where the resonant energy decreases (black line) because of a stepwise-increasing undulator K value. The common simulation parameters are shown in Table 2.

Table 2: Genesis Simulation Parameters

Quantity	Value	Units
energy ( $\gamma_0 m_e c^2$ )	3.969	GeV
energy spread ( $\sigma_\gamma m_e c^2$ )	3.5, 7.0	MeV
transverse emittance	0.6	$\mu\text{m}$
photon energy (nominal)	700	eV
undulator period	3.0	cm
starting K value	3.50	
ending K value	3.52	
undulator gap K value	0.0	
undulator modules	6	
peak current	5.5	kA
phase space	ideal Gaussian beam	
Pierce Parameter ( $\rho$ )	$2.2 \times 10^{-3}$	

The difference between the two simulations is in energy spread. The top simulation in Fig. 2 uses a 3.5 MeV rms energy spread, while the bottom simulation uses a 7.0 MeV energy spread. In both simulations bunching grows at a range of energies between what is resonant at the start and end of the undulator line (693 eV - 700 eV).

In the 3.5 MeV energy spread simulation, bunching grows at a wide range of frequencies, peaking in intensity at a frequency in the middle of the reverse taper range. This

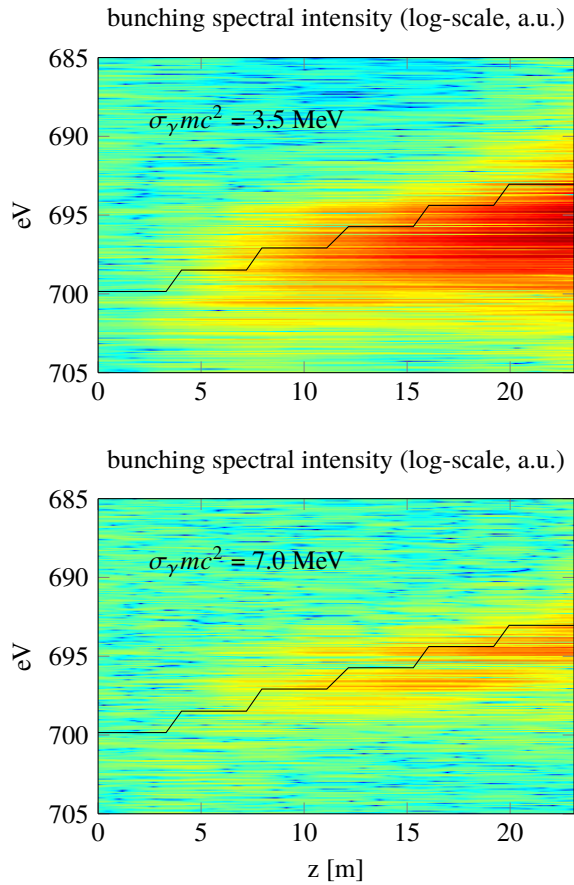


Figure 2: The bunching spectral intensity evolves as a function of distance along the undulator line in two time dependent Genesis simulations:  $\sigma_\gamma mc^2 = 3.5$  MeV (top), and 7.0 MeV (bottom). The spectral intensity is plotted in arbitrary units but on the same scale in the top and bottom simulations. The black line traces the energy resonant to the reverse tapered undulator at a particular location.

is consistent with the theoretical expectation for a slowly varying reverse taper [3]. In the 7.0 MeV case, however, bunching growth is less successful. Bunching initiated at a particular frequency early on in the undulator line cannot be amplified in undulator segments with a larger detune. This is a result of the limitation in Eq. (24), which can be rewritten in a more illuminating form

$$E_{hv,\max}(z) = 2E_{hv_0} \left( \rho^3 \frac{\gamma_0^2}{\sigma_\gamma^2} + \frac{\Delta\gamma(z)}{\gamma_0} \right) + E_{hv_0}, \quad (31)$$

where  $E_{hv_0} = 700$  eV,  $\Delta\gamma(z)/\gamma_0$  reaches a minimum of  $-0.0049$  at the end of the undulator line, and other parameters are given in Table 2.  $E_{hv,\max}(z)$  is the maximum photon energy that will experience exponential growth due to the FEL instability. Plugging in the two different energy spread values, this means

$$E_{hv,\max}(\text{end}) = \begin{cases} 714 \text{ eV}, & \sigma_\gamma mc^2 = 3.5 \text{ MeV} \\ 698 \text{ eV}, & \sigma_\gamma mc^2 = 7.0 \text{ MeV} \end{cases} \quad (32)$$

$$(33)$$

at the end of the undulator line. In the high energy spread case, no FEL growth will take place above 698 eV. This matches the drop in bunching spectral intensity in the bottom panel if Fig. 2 above 698 eV in the final undulator segment. No such constraint on FEL growth is placed on the 3.5 MeV energy spread simulation, all relevant frequencies are amplified.

## CONCLUSION

The electron beam energy spread places a strong constraint on the FEL field growth at large detunes from resonance. This in turn limits the maximum achievable bunching to field strength ratio. A high bunching to field strength ratio is critical for successful operation of a helical undulator like the Delta undulator following a reverse tapered planar undulator line. The energy spread of LCLS in the soft x-ray regime is large enough for this effect to limit the power contrast seen in the Delta undulator, restricting the maximum achievable degree of polarization.

## APPENDIX: LASER HEATER DISTRIBUTION

A laser heater is used at LCLS to combat the microbunching instability by increasing the slice energy spread of the beam. The electron energy distribution exiting a laser heater depends on the initial distribution and the laser and electron beam transverse matching. In this section the initial energy distribution is assumed to be negligible relative to the energy modulation from the laser heater.

For a beam with zero initial energy spread, a transverse beam size of  $\sigma_x$ , and a laser energy modulation of  $\Delta\bar{\eta}_L(r) \sin(k_L z)$  at the laser wavenumber  $k_L$ , the post-laser heater distribution function is

$$V(r, z, \bar{\eta}) = \delta(\bar{\eta} - \Delta\bar{\eta}_L(r) \sin k_L z) \frac{1}{2\pi\sigma_x^2} e^{-r^2/2\sigma_x^2}, \quad (A1)$$

where  $\delta$  is the Dirac's delta function and the radial dependence of the energy modulation is

$$\Delta\bar{\eta}_L(r) = 2\zeta e^{-r^2/4\sigma_r^2} \quad (A2)$$

for an interaction with a maximum energy modulation of  $2\zeta$ . As in previous sections, the scale factor  $2\zeta$  will dictate the width of the energy distribution. The factor of 2 is used to set the resultant energy distribution to an rms width of  $\zeta$ . The distribution in Eq. (A1) can be integrated over the transverse and longitudinal coordinates to find the energy distribution function,

$$V(\bar{\eta}) = \int 2\pi r dr \int V(r, z, \bar{\eta}) dz \quad (A3)$$

$$= \frac{1}{2\pi\zeta} \int_0^{2B \log(2\zeta/\bar{\eta})} \frac{e^{-x}}{\sqrt{e^{-B^2x} - \bar{\eta}^2/4\zeta^2}} dx \quad (A4)$$

where  $B = \sigma_r/\sigma_x$  and the assumption  $B \geq 1$  has been applied. This integral can be rewritten in terms of Hypergeometric functions, but it is more instructive to examine two

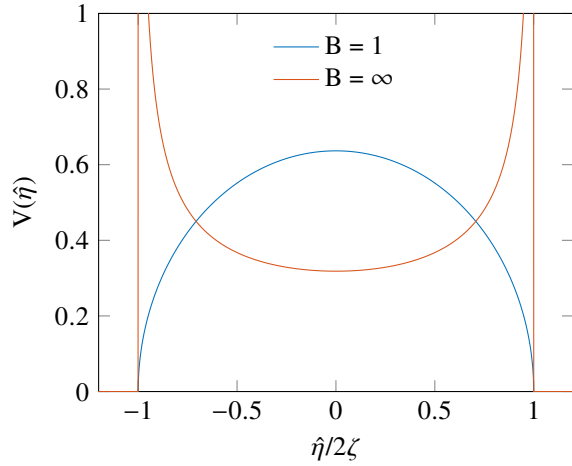


Figure 3: The energy distribution from a matched beam ( $B = 1$ ) and an unmatched beam ( $B = \infty$ ) exiting the laser heater. By assuming the energy spread entering the laser heater is negligibly small, exact expressions for these distributions are given by Eqs. (A5, A6).

special cases,

$$V(\bar{\eta}) = \begin{cases} \frac{1}{\pi\zeta} \left(1 - \bar{\eta}^2/4\zeta^2\right)^{1/2}, & B = 1 \quad (\text{A5}) \\ \frac{1}{2\pi\zeta} \left(1 - \bar{\eta}^2/4\zeta^2\right)^{-1/2}, & B \rightarrow \infty. \quad (\text{A6}) \end{cases}$$

These distributions are shown in Fig. 3. The matched beam ( $B = 1$ ) case, where laser heaters typically operate, exhibits a centrally peaked and relatively narrow distribution. We therefore proceed to solve for the growth rate using this distribution.

Inserting Eq. (A5) into Eq. (19), it is clear that the growth rate is the solution to an algebraic equation

$$2\zeta^2(\hat{\mu} - \hat{\nu}) = \left(1 - 4\frac{\zeta^2}{\hat{\mu}^2}\right)^{-1/2} - 1. \quad (\text{A7})$$

The roots of this polynomial are easily calculated with symbolic processing software. As before, we seek the upper limit on  $\hat{\nu}$  for a given energy spread  $\zeta$ . The upper limit is the solution to the equation  $\text{Im}(\hat{\mu}) = 0$ . As before, this implies  $\hat{\mu} = 0$ , and the boundary is

$$\hat{\nu} \leq \frac{1}{2\zeta^2}. \quad (\text{A8})$$

This boundary is plotted above the solution to Eq. (A7) in Fig. 4. The rms energy spread of Eq. (A5) and the Gaussian distribution in Eq. (20) are  $\zeta$ . The detune limit is a factor of two more stringent in the laser heater case for the same rms spread.

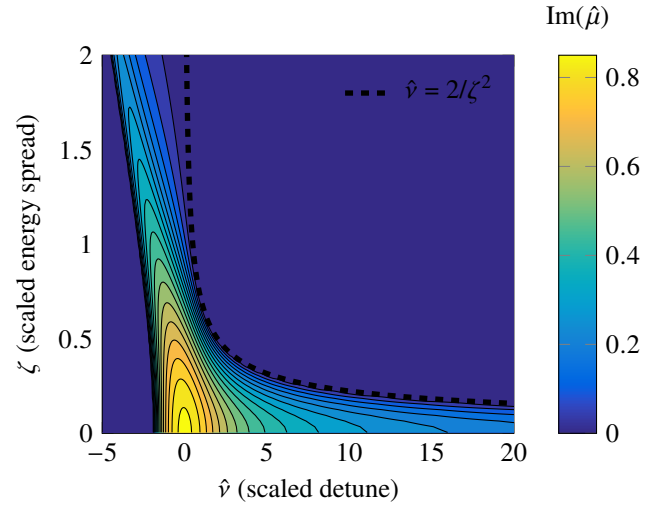


Figure 4: A numerical calculation of the growth rate  $\text{Im}(\hat{\mu})$  as a function of the scaled detune  $\hat{\nu}$  and the scaled rms energy spread  $\zeta$ . In contrast to Fig. 1, here the growth rate is calculated assuming a laser heater energy distribution given by Eq. (A5). The upper limit on the scaled detune is given by Eq. (A8).

## REFERENCES

- [1] A. B. Temnykh. “Delta undulator for Cornell energy recovery linac.” In: *Phys. Rev. ST Accel. Beams* 11 (12 Dec. 2008), p. 120702.
- [2] E. A. Schneidmiller and M. V. Yurkov. “Obtaining high degree of circular polarization at x-ray free electron lasers via a reverse undulator taper.” In: *Phys. Rev. ST Accel. Beams* 16 (11 Nov. 2013), p. 110702.
- [3] Z. Huang and G. Stupakov. “Free electron lasers with slowly varying beam and undulator parameters.” In: *Phys. Rev. ST Accel. Beams* 8 (4 Apr. 2005), p. 040702.
- [4] B. Pfau et al. “Ultrafast optical demagnetization manipulates nanoscale spin structure in domain walls.” In: *Nature communications* 3 (2012), p. 1100.
- [5] T. Wang et al. “Femtosecond Single-Shot Imaging of Nanoscale Ferromagnetic Order in Co/Pd Multilayers Using Resonant X-Ray Holography.” In: *Phys. Rev. Lett.* 108 (26 June 2012), p. 267403.
- [6] U. Hergenhahn et al. “Photoelectron circular dichroism in core level ionization of randomly oriented pure enantiomers of the chiral molecule camphor.” In: *The Journal of Chemical Physics* 120.10 (2004), pp. 4553–4556.
- [7] H-D Nuhn et al. “R&D; Towards a Delta-Type Undulator for the LCLS.” In: *Presented at FEL 2013*. SLAC-PUB-15743. 2013.
- [8] Z. Huang et al. “Suppression of microbunching instability in the linac coherent light source.” In: *Phys. Rev. ST Accel. Beams* 7 (7 July 2004), p. 074401.